



Applied Energy Symposium and Forum, Renewable Energy Integration with Mini/Microgrids,
REM 2018, 29–30 September 2018, Rhodes, Greece

An AC OPF with voltage – frequency coupling constraints for addressing operational challenges of AC/DC microgrids

A. Oulis Rousis^{a,*}, I. Konstantelos^a, P. Fatouros^a, G. Strbac^a

^aImperial College London, Kensington Campus, London SW7 2AZ, United Kingdom

Abstract

This paper focuses on developing an appropriate optimization technique for solving the optimal operation problem of hybrid AC/DC microgrids. A non-linear mathematical formulation is deployed to solve the problem subject to the exhaustive set of constraints and equations pertaining to the operation of AC and DC networks. The proposed approach, being able to capture technical characteristics, such as voltage and frequency, through the detailed power flow algorithm, provides accurate solutions and therefore can address operational challenges of MGs. The approach is applied to a highly-generalizable microgrid comprising of AC and DC generators and loads, as well as storage technologies in order to demonstrate the benefits. The simulation results demonstrate how voltage and frequency are effectively captured across the whole network via the utilised formulation and the power flow through the interlinking converter is associated with frequency (i.e. 49-51 Hz) and voltage variation (i.e. 0.95-1.05 p.u.).

© 2019 The Authors. Published by Elsevier Ltd.

This is an open access article under the CC-BY-NC-ND license (<https://creativecommons.org/licenses/by-nc-nd/4.0/>)

Selection and peer-review under responsibility of the scientific committee of the Applied Energy Symposium and Forum, Renewable Energy Integration with Mini/Microgrids, REM 2018.

Keywords: AC/DC microgrid, Microgrid operation, AC optimal power flow

1. Introduction

Microgrids (MGs) have lately attracted great attention, and it has become apparent that they will play a critical role in the development of future energy systems worldwide due to the clear benefits they provide over the traditional top-down, radial network philosophy [1]. Although great uncertainty surrounds the prevailing MG architectures that will

* Corresponding author.

E-mail address: a.oulis-rousis16@imperial.ac.uk

emerge, building-scale and local-aggregator MGs are expected to become common in the coming decades [2]. In both cases, the MG operator can have access to a plethora of different resources; AC and DC generators, such as wind turbines and PV plants respectively, AC or DC loads (e.g. electric vehicles), and various types of Energy Storage (ES) technologies (e.g. fuel cells and supercapacitors) [3]. The different technical characteristics of these resources pose challenges towards investigating their associated benefits. Thus, detailed modelling is considered essential to accurately capture the components' behaviour, which can effectively enable investigation of their benefits. For addressing such operational challenges, an AC power flow formulation is needed that involves highly non-linear constraints. Additionally, it is important to investigate the behaviour of the system during contingencies, as this can reveal problematic areas. Contingencies increase the problem's dimensionality, which in overall leads to a larger problem size, as it will be revealed in the sections below. Finally and with reference to hybrid AC/DC MGs that offer additional benefits due to the elimination of multiple conversion stages, the energy exchange between the AC and DC subgrids should also be associated with a set of technical constraints that allow voltage and frequency measures to be correlated between the two subnetworks [4]. The above considerations result in a large Non-Linear Program (NLP).

The proposed method is applied to a highly-generalizable hybrid MG case study consisting of AC wind turbine generators and DC photovoltaic arrays. On the demand side, both typical DC loads (e.g. electric vehicles) and AC loads (e.g. water pumps) are considered. As far as the storage devices are concerned, technologies with complementary operating characteristics are considered (e.g. Li-ion fuel cells, lead-acid batteries, supercapacitors). Through the extensive analysis of this case study, the sections following hereafter address fundamental modeling and conceptual challenges pertaining to the operation of the emerging hybrid MG paradigm.

2. Optimal of a Hybrid AC/DC MG through a Detailed AC OPF

The AC Optimal Power Flow (OPF), introduced in this section, is utilized for assessing the operational aspects of the problem, so that the total system cost is minimized; i.e. the summation of any generation cost including penalisation for involuntary load shedding of the MG. In mathematical terms, the objective function of the problem is given by (1). The *first term* denotes the generation cost. The *second term* is included to account for penalization in case the optimizer proceeds with load shedding. Finally, the *third term* is included to avoid infeasibilities, and in practice is modelled as an artificial, very expensive generator.

$$\begin{aligned}
 F = & \sum_{c \in C} \sum_{t \in T} \sum_{g \in G} c_g \cdot P(g, t, c) + \\
 & \sum_{c \in C} \sum_{t \in T} \sum_{b \in L_{bus}} c_{ls} \cdot (P_{loadshed}(b, t, c) + Q_{loadshed}(b, t, c)) + \\
 & \sum_{c \in C} \sum_{t \in T} \sum_{b \in G_{bus}} c_{os} \cdot (P_{overstack}(b, t, c) + Q_{overstack}(b, t, c))
 \end{aligned} \tag{1}$$

The optimization problem can be posed as a minimization problem, i.e. $\min(F)$, subject to the constraints represented by (2) - (8). Specifically, (2) - (4) introduce the operational constraints of the MG, while (5) - (8) correspond to the generator- and storage-relevant constraints. The equations shown below refer to the AC network, however as explained this formulation has been developed to provide an OPF solution for both an AC and a DC network. Therefore, in the developed model equations (2), (3), (5), (7) and (8) have been duplicated and accordingly modified to also account for the DC subnetwork [14], [15]. The equations are solved following a unified approach, according to which the AC and DC subproblems are solved simultaneously [5].

$$V_{min} \leq V(b, t, c) \leq V_{max} \quad \forall c \in C, \forall t \in T, \forall b \in N_{bus} \tag{2}$$

$$\max(S(i, t, c)) \leq S_i^{lim} \quad \forall c \in C, \forall t \in T, \forall i \in N_{br} \tag{3}$$

$$|\delta(b, t, c) - \delta(p, t, c)| \leq \delta^{lim} \quad \forall c \in C, \forall t \in T, \forall b, p \in N_{bus} \tag{4}$$

$$P_{g,min} \leq P(g, t, c) \leq P_{g,max} \quad \forall c \in C, \forall t \in T, \forall g \in N_g \tag{5}$$

$$Q_{g,min} \leq Q(g, t, c) \leq Q_{g,max} \quad \forall c \in C, \forall t \in T, \forall g \in N_g \tag{6}$$

$$0 \leq S^d(b, t, c), S^c(b, t, c) \leq S_b^{max} \quad \forall c \in C, \forall t \in T, \forall b \in S_{bus} \tag{7}$$

$$ES(b, t, c) = ES(b, t - 1, c) + (\eta_b \cdot S^c(b, t, c) - S^d(b, t, c)) \cdot \Delta t \quad \forall c \in C, \forall t \in T - \{1\}, \forall b \in S_{bus} \tag{8}$$

Equations (9) and (10) represent the active and reactive power balance equations at each bus b , where $P_b^{ex}(t)$ and $Q_b^{ex}(t)$ are given by (11) and (12), which are the classical equations pertaining to power flow problems.

$$S^d(b, t, c) - S^c(b, t, c) + \sum_{g \in NG_b} P(g, t, c) + P_{loadshed}(b, t, c) = P^{ex}(b, t, c) + P_{load}(b, t, c) + P_{overslack}(b, t, c) + P_{ic}(t, c) \quad (9)$$

$$\sum_{g \in NG_b} Q(g, t, c) + Q_{loadshed}(b, t, c) = Q^{ex}(b, t, c) + Q_{load}(b, t, c) + Q_{overslack}(b, t, c) + Q_{ic}(t, c) \quad (10)$$

$$P^{ex}(b, t, c) = \sum_{\substack{p \in N_{bus} \\ \in T, \forall b \in N_{bus}}} V(b, t, c) \cdot V(p, t, c) \cdot (G_{bp} \cos \delta_{bp}(t, c) + B_{bp} \sin \delta_{bp}(t, c)) \forall c \in C, \forall t \quad (11)$$

$$Q^{ex}(b, t, c) = \sum_{\substack{p \in N_{bus} \\ \in T, \forall b \in N_{bus}}} V(b, t, c) \cdot V(p, t, c) \cdot (G_{bp} \sin \delta_{bp}(t, c) - B_{bp} \cos \delta_{bp}(t, c)) \forall c \in C, \forall t \quad (12)$$

Note that equations (9) and (10) include the terms $P_{ic}(t, c)$ and $Q_{ic}(t, c)$ respectively, which represent the power flow through the interlinking converter connecting the AC and DC grids. $P_{ic}(t, c)$ and $Q_{ic}(t, c)$ are accordingly determined by (13) and (14), which correspond to a droop control strategy implemented in the converter [19], [28].

$$P_{ic} = -\frac{1}{\gamma_p} \cdot \Delta e \quad (13)$$

$$Q_{ic} = -\frac{1}{\gamma_q} \cdot \Delta e \quad (14)$$

Local measurements of frequency at the AC terminal and determination of the DC voltage at the DC terminal in the two ends of the interlinking converter are utilised to effectively calculate Δe , which represents the difference between the frequency and DC voltage. To allow comparison of the latter two measures, a normalisation procedure is followed to bring the measurements in a per unit basis (what is called *feature scaling* in statistics), as described by (15) and (16). These equations convert the given dataset in values within the range [-1,1]. The error, Δe , is continuously calculated over the time horizon. A negative value of Δe corresponds to power transfer from the DC subnetwork to the AC, and vice versa.

$$\hat{\omega} = \frac{2 \cdot \omega - (\omega_{max} + \omega_{min})}{\omega_{max} - \omega_{min}} \quad (15)$$

$$\hat{V}_{dc} = \frac{2 \cdot V_{dc} - (V_{dc,max} + V_{dc,min})}{V_{dc,max} - V_{dc,min}} \quad (16)$$

This procedure is an effective way of coupling the voltage and frequency between the two networks and eventually associating the exchanging power flows to these values. Therefore, the process introduces a means of capturing measures relevant to dynamic phenomena, and it enhances the utilisation of the OPF algorithm during transient states.

3. Description of Case Study Network

The methodology shown in the previous section has been applied to the highly-generalizable MG illustrated in Fig. 1. The network consists of an AC wind turbine and a DC photovoltaic array each with a capacity of 100 kW, as well as two conventional generators (i.e. one at each subnetwork) each with a capacity of 150 kW. On the demand side, both typical DC loads (e.g. electric vehicles) and AC loads (e.g. water pumps) are considered (see Fig. 2 more information). As far as the storage devices are concerned, the AC side includes a low energy – low power battery (i.e. 50 kW/200 kWh), while the DC side a medium power – high energy battery (100 kW/2000 kWh) [6].

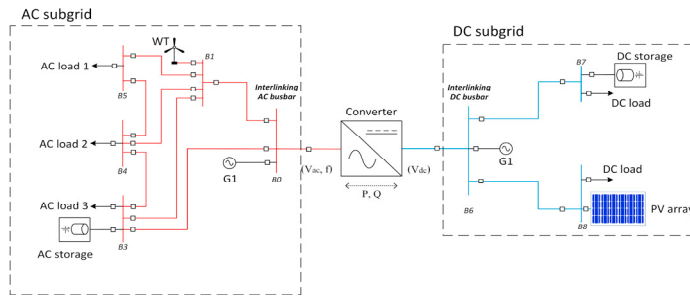


Fig. 1. Case study hybrid AC/DC network

3.1. Simulation results

This section presents the simulation results utilising the tool described in Section 2. For the analysis, we consider a contingency occurring from 13:00 to 15:00 that leads the interlinking converter to be out of service for this 2-hour timeslot, as shown in Fig. 3. For the 2-hour timeslot of the contingency the power is equal to 0. Note that active power takes negative values, which indicates that the AC subnetwork is supplying power to the DC subnetwork. This is expected, since the AC subnetwork includes the wind turbine that generates power at all times.

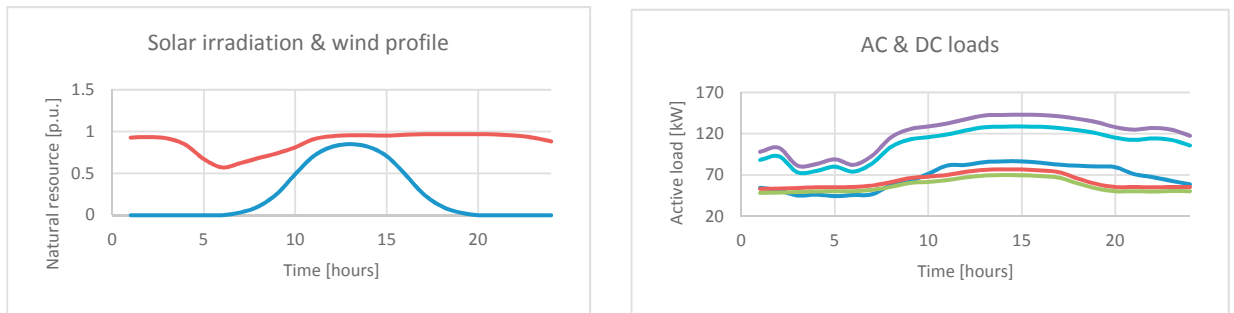


Fig. 2. Solar irradiation and wind profile (left) – AC and DC loads (right)

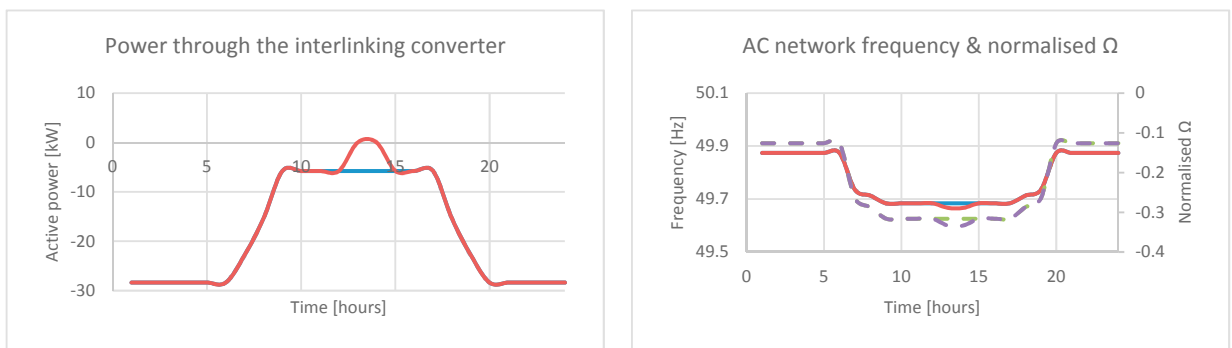


Fig. 3. Power flow through the interlinking converter with (red line) and without a contingency (blue line) (left) – AC network frequency and normalisation error (right).

From a technical perspective, the contingency has an effect on the AC network’s frequency, as depicted on the right side of Fig. 3 above. This indicates that the voltage-frequency coupling constraint introduced by equations (13) – (16) creates the conditions required to effectively measure frequency and couple it with active power changes occurring on the given network. This change in active power and consequently in frequency is captured through the simulation in the normalisation error, which drops to 0 during 13:00 – 15:00; this is as per equation (13).

It would be expected that during the contingency the optimiser would try to cover for the power deficit from amassing energy from the PV array or the DC storage. However, by observing Fig. 4 we can see no significant difference between the cases with and without the contingencies (i.e. red and blue lines respectively).

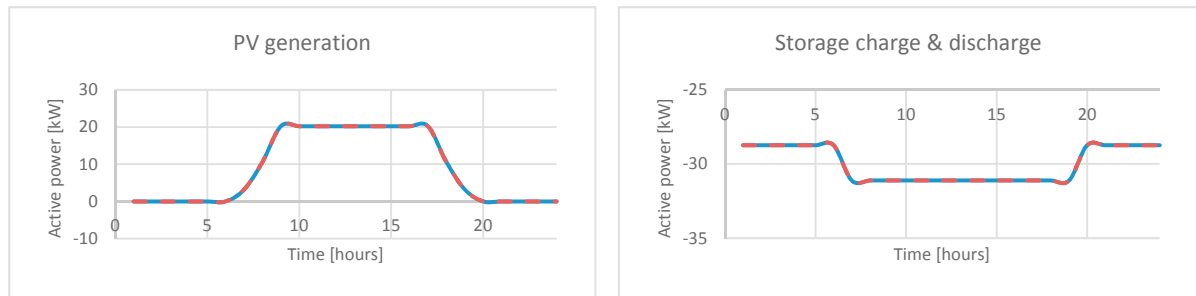


Fig. 4. PV generation (left) – DC-side storage device charging and discharging

This is because the model is constrained by technical parameters that do not allow more power to be transferred through the lines. Specifically, Fig. 5 illustrates the voltage of B6, the bus connecting the interlinking converter to the DC subnetwork. The permissible range for the voltage is $[0.9, 1.1]$. Bus B6 maintains its voltage at 0.9 p.u., and that is why no more power can flow through this bus (i.e. the only bus connecting the generators with one of the loads). Same applies to bus B7. Therefore, this explains why the PV array produces no more than 20 kW, even though its capacity is 100 kW, and the DC battery cannot discharge more than 31 kW. This is important, as typical energy management systems found in the literature would neglect this aspect allowing power to be transferred; this would lead to violation of technical requirements. Of course, this negatively impacts on the operational cost, as the surplus of load (i.e. approximately 5 kW) is shed for each of these two hours, significantly raising the operational cost.

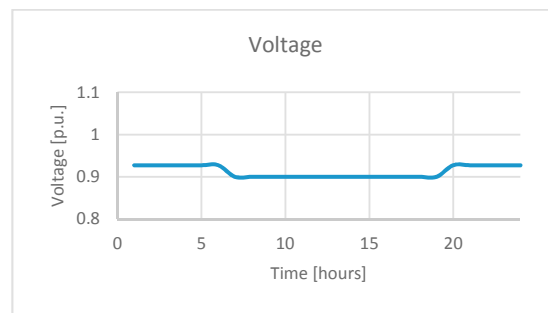


Fig. 5. Voltage profile of B6

4. Conclusions

This paper has presented a detailed AC OPF formulation for addressing the optimal operation of AC/DC MGs. A voltage – frequency coupling has been introduced as a means of capturing a technical measure from one subnetwork to the other. A normalisation procedure has been introduced which translates the admissible frequency and voltage ranges into the range $[-1, 1]$, hence it creates a per unit representation of these two measures. The results indicate that this becomes important, especially when an onerous contingency occurs as it allows operation without violating technical constraints. In the context of the future power system, where MGs will be connected to distribution systems offering services, the ability to capture all technical characteristics and abide with the imposed technical requirements will be a very significant factor. It is believed that this work will become even more critical by integrating relevant differential constraints, which will allow proper dynamic analysis of the MG system in much shorter timescales.

Nomenclature

δ^{lim}	Maximum allowable voltage angle variation between two buses
γ_p	Interlinking converter active power droop gain
γ_q	Interlinking converter reactive power droop gain
ω_{max}	Maximum permissible value of frequency ω
ω_{min}	Minimum permissible value of frequency ω
$C_{\text{ls/os}}$	Cost associated with load shedding/overslack
$P_{g,\text{max/min}}$	Maximum/minimum power of a generator g (active)
$Q_{g,\text{max/min}}$	Maximum/minimum power of a generator g (reactive)
$S(i)^{\text{lim}}$	Capacity limit of branch i
S_b^{max}	Maximum storage power
$V_{(\text{dc}),\text{max}}$	Maximum permissible (DC) AC voltage
$V_{(\text{dc}),\text{min}}$	Minimum permissible (DC) AC voltage
Δe	Error between the normalized frequency and the normalized DC voltage
$\delta_{bp}(t, c)$	Voltage angle difference between buses b, p at time t for contingency c
$ES(b, t, c)$	Energy content in storage in bus b at the end of the current time step for contingency c
$P(g, t, c)$	Active power generation of generator g at time t for contingency c
$P^{\text{ex}}(b, t, c)$	Active power exchange between considered bus b and other buses at time t for contingency c
$P_{\text{ic}}(t, c)$	Active power flow through the interlinking converter at time t for contingency c
$P_{\text{loadshed}}(b, t, c)$	Involuntary loss of active load at bus b at time t for contingency c
$P_{\text{load}}(b, t, c)$	Active load at bus b at time t for contingency c
$P_{\text{overslack}}(b, t, c)$	Overslack for active power at bus b at time t for contingency c
$Q(g, t, c)$	Reactive power generation of generator g at time t for contingency c
$Q^{\text{ex}}(b, t, c)$	Reactive power exchange between considered bus b and other buses at time t for contingency c
$Q_{\text{ic}}(t, c)$	Reactive power flow through the interlinking converter at time t for contingency c
$Q_{\text{loadshed}}(b, t, c)$	Involuntary loss of reactive load at bus b at time t for contingency c
$Q_{\text{load}}(b, t, c)$	Reactive load at bus b at time t for contingency c
$Q_{\text{overslack}}(b, t, c)$	Overslack for reactive power at bus b at time t for contingency c
$S^c(b, t, c)$	Storage charging into bus b at time t for contingency c
$S^d(b, t, c)$	Storage discharging from bus b at time t for contingency c
$V(b, t, c)$	Voltage at bus b at time t for contingency c

Acknowledgements

This research was funded by the Engineering and Physical Sciences Research Council grant number EP/N034570/1.

References

- [1] G. Strbac, N. Hatzigiorgiou, J. P. Lopes, C. Moreira, A. Dimeas, and D. Papadaskalopoulos, "Microgrids: Enhancing the Resilience of the European Megagrid," *IEEE Power and Energy Magazine*, vol. 13, no. 3, pp. 35–43, May–June 2015.
- [2] N. Hatzigiorgiou, "The Microgrids Concept," in *Microgrids: Architecture and Control*, 1, Wiley-IEEE Press, 2014, pp. 344–.
- [3] H. Xie, S. Zheng, and M. Ni, "Microgrid development in china: A method for renewable energy and energy storage capacity configuration in a megawatt-level isolated microgrid." *IEEE Electrification Magazine*, vol. 5, no. 2, pp. 28–35, June 2017.
- [4] G. AlLee and W. Tschudi, "Edison redux: 380 vdc brings reliability and efficiency to sustainable data centers," *IEEE Power and Energy Magazine*, vol. 10, no. 6, pp. 50–59, Nov 2012.
- [5] A. A. Eajal, M. A. Abdelwahed, E. F. El-Saadany, and K. Ponnambalam, "A unified approach to the power flow analysis of ac/dc hybrid microgrids," *IEEE Transactions on Sustainable Energy*, vol. 7, no. 3, pp. 1145–1158, July 2016.
- [6] X. Luo, J. Wang, M. Dooner, and J. Clarke, "Overview of current development in electrical energy storage technologies and the application potential in power system operation," *Applied Energy*, vol. 137, pp. 511–536, 2015.